

Extremum Seeking for Wind and Solar Energy Applications

Miroslav Krstic and Azad Ghaffari

Department of Mechanical and Aerospace Engineering
University of California, San Diego
La Jolla, CA 92093-0411
{krstic and aghaffari}@ucsd.edu

Sridhar Seshagiri

Department of Electrical and Computer Engineering
San Diego State University
San Diego, CA 92182-1309
seshagir@engineering.sdsu.edu

Abstract—Invented in 1922, extremum seeking (ES) is one of the oldest feedback methods. However, its purpose is not regulation but optimization. For this reason, applications of ES have often come from energy systems. The first noted publication on ES in the West is Draper and Li's application to spark timing optimization in internal combustion engines [1]. In the ensuing decades, ES has been applied to gas turbines and even nuclear fusion reactors. Renewable energy applications have brought a new focus on the capabilities of ES algorithms. In this article we present applications of ES in two types of energy conversion systems for renewable energy sources: wind and solar energy. In both areas the goal is maximum power point tracking (MPPT), i.e., the extraction of the maximum feasible energy from the system under uncertainty and in the absence of a priori modeling knowledge about the systems. For the wind energy conversion system (WECS) we perform MPPT by tuning the set point for the turbine speed using scalar ES. For the photovoltaic (PV) array system, we perform MPPT by tuning the duty cycles of the DC/DC converters employed in the system using multivariable ES. For the photovoltaic system we provide experimental results. (Abstract)

Keywords—energy harvesting; wind energy; solar energy; nonlinear dynamical systems; adaptive control; optimization; power control (key words)

I. INTRODUCTION

Increasing availability of energy storage devices motivates the effort to harvest maximum feasible power from renewable sources, particularly wind turbines (WTs) and photovoltaic (PV) systems. Renewable sources operate under a wide range of uncertain environmental parameters and disturbances. For example, uncertain quantities such as wind speed in WT and solar irradiance in PV modules affect the respective power maps and the maximum power points (MPPs). However, the power map is also a function of a control input—the turbine speed in WT and the terminal voltage in the PV modules. The power map of WT has a unique MPP with respect to turbine speed at each level of wind speed. Likewise, the power map of a PV module has a unique MPP with respect to terminal voltage at each level of solar irradiance.

The process of governing a WT or PV module to its MPP is known as maximum power point tracking (MPPT). The conventional perturb and observe (P&O) techniques do so by a combination of adding a step perturbation to the control signal and monitoring the direction of changes in power [2-8]. Most techniques derived from P&O are based on discrete analysis and require a delicate balance between the amplitude of the control input step perturbation and the possible changes in environmental parameters. Moreover, the sampling frequency needs to be carefully selected with respect to the response time

of the system to the step perturbation. Since the system is not linear, the sampling frequency is also a function of the step size and of the magnitude of changes in environmental parameters [2-4, 6].

Extremum seeking (ES) is an attractive alternative to P&O techniques for solving MPPT problems in wind and solar systems. As a model-free, real-time optimization approach, ES is well suited for systems with unknown dynamics or those that are affected by high levels of uncertainty or external dynamics, like WT and PV systems. Similar to P&O techniques, ES employs perturbations [9-21]. However, instead of employing a discrete step perturbation, ES uses a continuous oscillatory perturbation, also known as a “probing function.” More importantly, ES does not merely monitor the direction of the output response but exploits the measured response to estimate the gradient of the power map and update the control input in proportion to the gradient of the power map [9].

ES has the dual benefit of rigorously provable convergence [9-13] and the simplicity of hardware implementation [14-21]. In addition to a probing signal, the ES algorithm employs only an integrator, as well as optional high-pass and low-pass filters. The amplitude and frequency of the probing function in ES influence the precision of the MPPT algorithm. However, the frequency selection is not as complicated as the selection of the sampling frequency in P&O technique. For dynamic systems, it is enough to select the ES probing frequency reasonably smaller than the highest frequency that can pass the system without significant attenuation.

ES guides the system to its MPP regardless of the magnitude of changes in environmental parameters, as long as the changes are slow. While the power map shape defines the convergence rate of the conventional gradient-based ES, we also present in this article more sophisticated schemes like the Newton-based ES [13] to alleviate the issue of unsymmetrical transients.

In some cases we need an inner-loop control to achieve desired closed-loop performance, for example, for speeding up the convergence rate and alleviating magnetic saturation in WT systems [21]. Combining a discrete MPPT method such as P&O with a continuous inner-loop control creates a hybrid system that needs careful parameter selection, particularly the sampling period and perturbation amplitude [22]. In contrast, ES can be applied without modifications to any system with a stabilizing inner-loop control.

When dealing with a multivariable power map, such as a cascade PV configuration with one converter per module, using a decentralized MPPT architecture is not the most efficient option. For multivariable MPPT, the complexity of

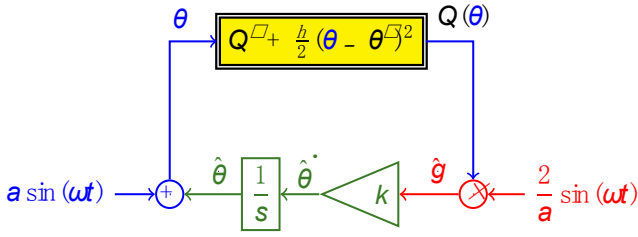


Fig. 1: The simplest perturbation-based ES scheme for a quadratic single-input map.

P&O algorithms increases dramatically with the size of the input vector. In contrast, ES trivially extends to multivariable MPPT, with only a few restrictions in selecting the probing frequencies [20]. Furthermore, with ES we have the option of employing the algorithm's Newton-based version to achieve transients that are symmetric relative to the peak of the MPP and uniform in speed for multiple modules [19].

The rest of this paper is organized as follows. In Section II we introduce ES for scalar static maps and then for dynamic systems with multivariable maps. We present both gradient- and Newton-based schemes. In Section III, we combine the scalar ES with a nonlinear inner-loop control developed from field-oriented control (FOC) to achieve power control and optimization in WT. We present simulation results to show the effectiveness of the proposed algorithm. In Section IV we present multivariable MPPT based on ES for PV systems. We verify the validity of the proposed algorithms with experimental results.

II. THE BASICS OF EXTREMUM SEEKING

Many versions of ES exist, with various approaches to the analysis of their stability. The most common version employs perturbation signals for the purpose of estimating the gradient of the unknown map that is being optimized [9]. To understand the basic idea of ES, it is best to first consider the case of a static single-input map of the quadratic form, as shown in Fig. 1, $Q(\theta) = Q^* + \frac{h}{2}(\theta - \theta^*)^2$, where Q^* , h , θ^* are all unknown. At the optimal point we have

$$\frac{\partial Q}{\partial \theta}(\theta^*) = 0, \quad \frac{\partial^2 Q}{\partial \theta^2}(\theta^*) = h. \quad (1)$$

The user has to only know the sign of h , namely, whether the quadratic map has a maximum or a minimum, and has to choose the adaptation gain k such that $\text{sgn}(k) = -\text{sgn}(h)$. The user has to also choose the frequency ω as relatively large compared to a , k , and h .

Three different θ s appear in Fig. 1: θ^* is the unknown optimizer of the map, $\hat{\theta}(t)$ is the real-time estimate of θ^* , and $\theta(t)$ is the actual input into the map. The actual input $\theta(t)$ is based on the estimate $\hat{\theta}(t)$ but is perturbed by the signal $a \sin \omega t$ for the purpose of estimating the unknown gradient $h(\theta - \theta^*)$ of the map $Q(\theta)$. The estimate $\hat{\theta}(t)$ is generated with the integrator $1/s$ with the adaptation gain k controlling the speed of estimation.

The ES algorithm is successful if the error between the estimate $\hat{\theta}(t)$ and the unknown θ^* , namely the signal

$$\tilde{\theta}(t) = \hat{\theta}(t) - \theta^* \quad (2)$$

converges towards zero. Based on Fig. 1, the estimate is governed by the differential equation $\dot{\hat{\theta}} = \frac{2k}{a} \sin(\omega t) Q(\theta)$, which means that the estimation error is governed by

$$\frac{d\tilde{\theta}}{dt} = \frac{2k}{a} \sin(\omega t) \left[Q^* + \frac{h}{2} (\tilde{\theta} + a \sin(\omega t))^2 \right]. \quad (3)$$

Expanding the right-hand side one obtains

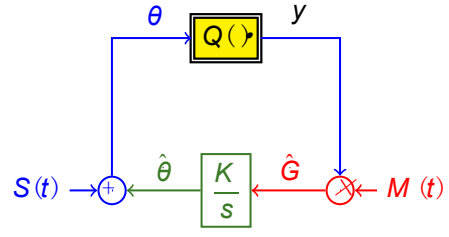


Fig. 2: The ES algorithm for a multivariable map.

$$\frac{d\tilde{\theta}(t)}{dt} = \frac{2k}{a} Q^* \underbrace{\sin(\omega t)}_{\text{mean}=0} + kah \underbrace{\sin^3(\omega t)}_{\text{mean}=0} + k \frac{h}{a} \underbrace{\sin(\omega t)}_{\text{fast, mean}=0} \underbrace{\tilde{\theta}^2}_{\text{slow}} + 2kh \underbrace{\sin^2(\omega t)}_{\text{fast, mean}=\frac{1}{2}} \tilde{\theta}. \quad (4)$$

A theoretically rigorous time-averaging procedure allows replacing the above sinusoidal signals by their means, yielding the ‘‘average system’’

$$\frac{d\tilde{\theta}^{\text{ave}}}{dt} = \frac{<0}{k\hbar} \tilde{\theta}^{\text{ave}} \quad (5)$$

which is exponentially stable. For a sufficiently large ω , if the initial estimate $\hat{\theta}(0)$ is sufficiently close to the unknown θ^* , then the input $\theta(t)$ exponentially converges to a small interval around the unknown θ^* and, consequently, the output $Q(\theta(t))$ converges to the vicinity of the optimal output Q^* .

A. ES for Multivariable Static Maps

For static maps, ES extends in a straightforward manner from the single-input case shown in Fig. 1 to the multi-input case shown in Fig. 2. The algorithm measures the scalar signal $y(t) = Q(\theta(t))$, where $Q(\cdot)$ is an unknown map whose input is the vector $\theta = [\theta_1 \theta_2 \cdots \theta_n]^T$. The gradient is estimated with the help of the signals

$$S(t) = [a_1 \sin(\omega_1 t) \cdots a_n \sin(\omega_n t)]^T \quad (6)$$

$$M(t) = \left[\frac{2}{a_1} \sin(\omega_1 t) \cdots \frac{2}{a_n} \sin(\omega_n t) \right]^T \quad (7)$$

with nonzero perturbation amplitudes a_i and with a gain matrix K that is diagonal. To guarantee convergence, the user should choose $\omega_i \neq \omega_j$. This is a key condition that differentiates the multi-input case from the single-input case. In addition, for simplicity in the convergence analysis, the user should choose ω_i/ω_j as rational and $\omega_i + \omega_j \neq \omega_k$ for distinct i, j , and k .

If the unknown map is quadratic, namely, $Q(\theta) = Q^* + \frac{1}{2}(\theta - \theta^*)^T H (\theta - \theta^*)$, the averaged system is

$$\dot{\tilde{\theta}} = KH\tilde{\theta}, \quad H = \text{Hessian}. \quad (8)$$

If, for example, the map $Q(\cdot)$ has a locally quadratic peak (which implies $H = H^T < 0$), and if the user chooses the elements of the diagonal gain matrix K as positive, the ES algorithm is guaranteed to be locally convergent. However, the convergence rate depends on the unknown Hessian H . This weakness of the gradient-based ES algorithm is removed with the Newton-based ES algorithm.

B. ES for Dynamic Systems

ES extends in a relatively straightforward manner from static maps to dynamic systems, provided the dynamics are stable and the algorithm's parameters are chosen so that the algorithm's dynamics are slower than those of the plant. The algorithm is shown in Fig. 3.

The technical conditions for convergence in the presence of dynamics are that the equilibria $x = l(\theta)$ of the system $\dot{x} = f(x, \alpha(x, \theta))$, where $\alpha(x, \theta)$ is the control law of an internal feedback loop, are locally exponentially stable

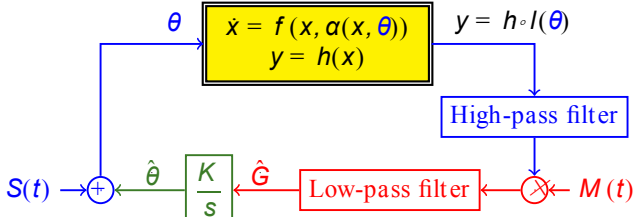


Fig. 3: The ES algorithm in presence of dynamics.

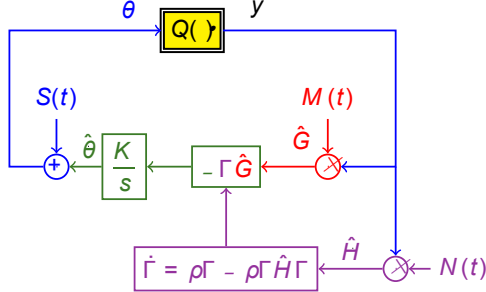


Fig. 4: A Newton-based ES for a static map.

uniformly in θ and that, given the output map $y = h(x)$, there exists at least one $\theta^* \in \mathbb{R}^n$ such that $\frac{\partial}{\partial \theta}(h \circ l)(\theta^*) = 0$ and $\frac{\partial^2}{\partial \theta^2}(h \circ l)(\theta^*) = H < 0, H = H^T$. The aforementioned criteria to select the ES parameters for a static map are still valid. Adding the inner control affects the probing frequency and the band-pass of the filters.

C. Newton ES Algorithm for Static Map

A Newton version of the ES algorithm, shown in Fig. 4, ensures that the convergence rate is user-assignable, rather than being dependent on the unknown Hessian of the map [13].

The elements of the demodulating matrix $N(t)$ for generating the estimate of the Hessian are given by

$$\begin{aligned} N_{ii}(t) &= \frac{16}{a_i^2} \left(\sin^2(\omega_i t) - \frac{1}{2} \right) \\ N_{ij}(t) &= \frac{4}{a_i a_j} \sin(\omega_i t) \sin(\omega_j t). \end{aligned} \quad (9)$$

The multiplicative excitation $N(t)$ helps to generate the estimate of the Hessian $\frac{\partial^2}{\partial \theta^2} Q(\theta)$ as $\hat{H}(t) = N(t)y(t)$. The Riccati matrix differential equation $\Gamma(t)$ generates an estimate of the Hessian's inverse matrix, avoiding matrix inversions of Hessian estimates that may be singular during the transient.

For a quadratic map, the averaged system in error variables $\tilde{\theta} = \hat{\theta} - \theta^*, \tilde{\Gamma} = \Gamma - H^{-1}$ is

$$\begin{aligned} \frac{d\tilde{\theta}^{\text{ave}}}{dt} &= -K\tilde{\theta}^{\text{ave}} - K \underbrace{\tilde{\Gamma}^{\text{ave}} H \tilde{\theta}^{\text{ave}}}_{\text{quadratic}} \\ \frac{d\tilde{\Gamma}^{\text{ave}}}{dt} &= -\rho\tilde{\Gamma}^{\text{ave}} - \underbrace{\rho\tilde{\Gamma}^{\text{ave}} H \tilde{\Gamma}^{\text{ave}}}_{\text{quadratic}}. \end{aligned} \quad (10)$$

Since the eigenvalues are determined by K and ρ , and are therefore independent of the unknown H , the (local) convergence rate is user-assignable.

In the next section we apply the scalar gradient-based ES to MPPT of a WT with an inner-loop control.

III. WIND ENERGY CONVERSION SYSTEMS

A schematic of a wind energy conversion system (WECS) including wind turbine (WT), induction generator (IG), and matrix converter (MC) is shown in Fig. 5. Wind turbines work in four different regions as depicted in Fig. 6. In Region I, the wind speed is too low for the turbine to generate power. Region II, also called the sub-rated power region, lies between the cut-in speed and rated speed. Here the generator operates at below rated power. The theoretical shape of this curve reflects the basic law of power production, where power is proportional to the cube of the wind speed. In Region III, the turbine limits the power output; this occurs when the wind is sufficient for the turbine to reach its rated output power. Region IV is the period of stronger winds, where the power in the wind is so great that it could be detrimental to the turbine, so the turbine shuts down [22].

The wind power available on the blade impact area is defined as

$$P_w = 2\rho_a A V_w^3, \quad A = \pi R^2, \quad (11)$$

where R is the blade length, ρ_a is air density, and V_w is wind speed. For Region II MPPT, assuming zero blade pitch angle, the turbine power is related to the wind power as

$$P_t = \omega_t T_t = C_p(V_w, \omega_t) P_w, \quad (12)$$

where T_t is the rotor torque, ω_t is the turbine speed, and C_p is the non-dimensional power coefficient, which is a measure of the ratio of the turbine power to the wind power. The power coefficient is a function of wind speed and turbine speed.

The turbine speed can be used to change the power coefficient, C_p , which results in power control and optimization. The MPPT algorithm in sub-rated power region should be able to guide the WT to its MPP regardless of the variations of the wind speed. The power captured by the WT is

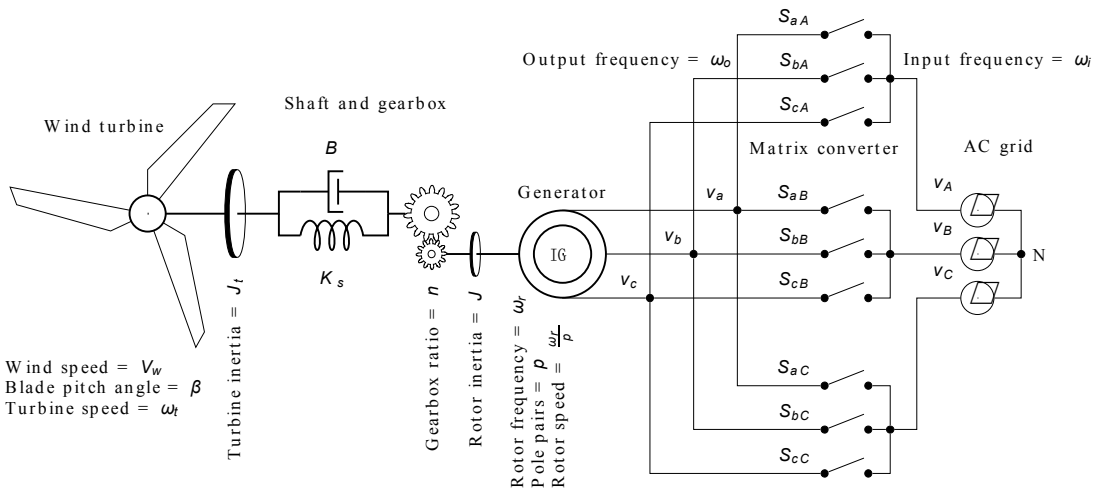


Fig. 5: WECS including WT, gear box, IG, and MC.

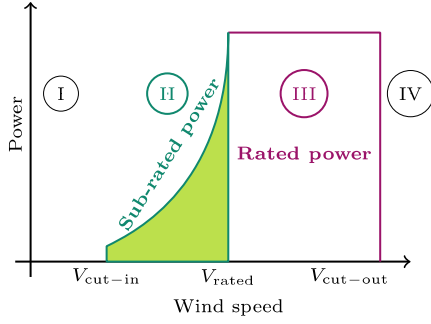


Fig. 6: Typical power curve of WT including four operating regions.

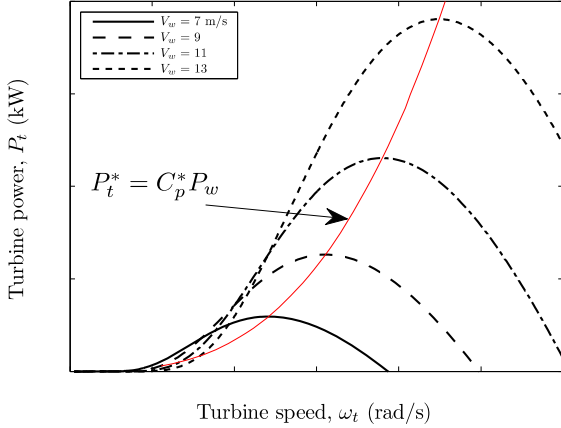


Fig. 7: Variation of the turbine power versus turbine speed for different wind speeds. The MPP moves on $C_p^* P_w$ curve which shows the characteristic of the sub-rated region of WECS.

defined by the wind speed, V_w , and the turbine speed, ω_t . However, the wind speed is a disturbance input and we can manipulate the turbine speed to govern the turbine power to its maximum power point (MPP) in sub-rated region. The variation of turbine power versus turbine speed is shown in Fig. 7 for different wind speeds. As shown in Fig. 7 under a constant wind speed the relevant power curve has a unique MPP, which is defined by a specific turbine speed. At the MPP the following observations are valid

$$\frac{\partial P_t}{\partial \omega_t}(\omega_t^*) = 0, \quad \frac{\partial^2 P_t}{\partial \omega_t^2}(\omega_t^*) = h < 0. \quad (13)$$

As shown in Fig. 5 the WT shaft is modeled as a spring-damper, and is connected to the electrical generator, which in this case is a squirrel-cage induction generator (SCIG), via a gearbox. Squirrel-cage IGs are relatively inexpensive, robust, and require little maintenance. When operated using vector control techniques, fast dynamic response, and accurate torque control is obtained. The generator is connected to the AC grid through a matrix converter (MC), which is a replacement for the conventional rectifier-inverter combination (AC-DC-AC), and steers the generator to its maximum power point (MPP) by controlling the electrical frequency of its stator of SCIG, which in turn leads to a speed variation in the turbine shaft. Matrix converters provide bidirectional power flow, sinusoidal input/output currents, and controllable input power factor [7, 24].

The input phase voltage of MC, $v_i = [v_A \ v_B \ v_C]^T$, which is connected to the AC grid, is given by

$$v_i = V_{im} \left[\cos(\theta_i) \ \cos\left(\theta_i - \frac{2\pi}{3}\right) \ \cos\left(\theta_i + \frac{2\pi}{3}\right) \right]^T, \quad (14)$$

where V_{im} is the peak value of the input voltage amplitude and

$$\theta_i = \int_0^t \omega_i dt \quad (15)$$

is the input electrical angle, where $\omega_i = 2\pi f_i$ is the input electrical frequency of the MC. Output voltage is $v_o = [v_a \ v_b \ v_c]^T$. It is the job of the MC to create local-averaged sinusoidal output phase voltage (the stator voltage of IG) and input phase current (the AC grid current)

$$v_o^{ave} = V_{om} \left[\cos(\theta_o) \ \cos\left(\theta_o - \frac{2\pi}{3}\right) \ \cos\left(\theta_o + \frac{2\pi}{3}\right) \right]^T, \quad (16)$$

where V_{om} is the peak value of the stator voltage amplitude and

$$\theta_o = \int_0^t \omega_o dt \quad (17)$$

is the output electrical angle where $\omega_o = 2\pi f_o$ is the stator electrical frequency. Stator electrical frequency, ω_o , and the peak value of the stator voltage amplitude, V_{om} , are control inputs and can be used for power control and optimization of the WECS.

A. Inner-Loop Control Design for WECS

In many motor drive systems, it is desirable to make the drive act as a torque transducer wherein the electromagnetic torque can nearly instantaneously be made equal to a torque command. In such a system, speed or position control is dramatically simplified because the electrical dynamics of the drive become irrelevant to the speed or position control problem. In the case of induction machine drives, such performance can be achieved using a class of algorithms collectively known as field-oriented control (FOC).

When flux amplitude is regulated to a constant reference value, and considering the fact that the dynamics of ω_t are considerably slower than the electrical dynamics, we can assume that the dynamics are linear, but during flux transient the system has nonlinear terms and it is coupled. This method can be improved by achieving exact input-output decoupling and linearization via a nonlinear state feedback that is not more complex than the conventional FOC [24].

One can manipulate stator voltage amplitude, V_{om} , and its frequency, ω_o , through the MC to obtain the desired closed-loop performance for WECS. By employing FOC idea we introduce an integrator and an auxiliary input, u_2 , to achieve input-output decoupling in WECS dynamics. Using one step of integration in front of V_{om} the extended equations of WECS are introduced as follows:

$$\dot{x} = f(x) + g_1 u_1 + g_2 u_2, \quad x \in \mathbb{R}^9, \quad u \in \mathbb{R}^2, \quad (18)$$

where $x = [i_\alpha \ i_\beta \ \lambda_\alpha \ \lambda_\beta \ \theta_o \ V_{om} \ \omega_r \ \tilde{\theta} \ \omega_t]^T$, where i_α and i_β are stator currents, λ_α and λ_β are rotor fluxes, $\tilde{\theta} = \theta_t - \frac{\theta_r}{pn}$,

$\theta_r = \int_0^t \omega_r dt$, ω_r is the rotor electrical frequency, $u_1 = \omega_o$ is the electrical frequency of the stator, u_2 is an auxiliary input (voltage amplitude rate) which generates the voltage amplitude of the stator.

From Fig. 7 we know that the turbine speed controls the power generation. Also we are interested in decoupling the rotor flux and electromagnetic torque to obtain the benefits of FOC. For these reasons, we introduce turbine speed, $y_1 = x_9$, and flux amplitude, $\eta_1 = x_3^2 + x_4^2$, as measurable outputs. Based on the selected outputs, we apply feedback linearization which results in the regulation of turbine speed, $\omega_t = y_1$, to its reference value ω_t^{ref} , while the amplitude of rotor flux, $|\lambda| = \sqrt{\eta_1}$, converges to its desired value, $|\lambda|^{ref}$.

B. Wind Turbine Power Optimization

To overcome challenges associated with the conventional power control and optimization algorithms and to remove the dependence of the MPPT algorithm on the system modeling

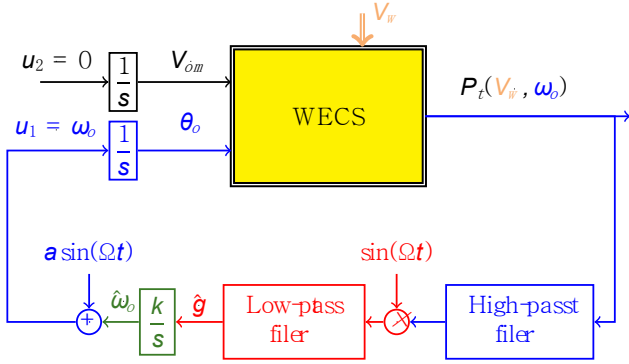


Fig. 8: The ES algorithm for MPPT of the WECS without the inner-loop control.

and identification, we propose an ES algorithm for MPPT of WECS. First we present ES without the inner-loop control to clarify the advantages of the inner-loop control on the closed-loop performance of the system.

In this paper we assume that we have access to turbine power measurements and we can manipulate the turbine speed through the MC. Furthermore, we do not have a model of the power coefficient or turbine power. But, we know that the turbine power map has one MPP under any wind speed.

The torque-speed characteristic of an induction machine is normally quite steep in the neighborhood of stator electrical frequency (synchronous speed), ω_o , and so the electrical rotor speed, ω_r , will be near the synchronous speed. This means that changing the reference value of the turbine speed, ω_t , which translates in variation of the electrical rotor speed eventually, results in changing the stator electrical frequency. Thus, by controlling the stator electrical frequency one can approximately control the turbine speed or vice versa. We can rewrite (13) as follows

$$\frac{\partial P_t}{\partial \omega_o}(\omega_o^*) = 0, \quad \frac{\partial^2 P_t}{\partial \omega_o^2}(\omega_o^*) = h' < 0. \quad (19)$$

A schematic of MPPT for WECS with extremum seeking without inner-loop nonlinear control is shown in Fig. 8. As mentioned in the last paragraph, the power is parameterized by ω_o , which is estimated by the ES loop. The other input for WECS which generates the voltage amplitude has been set to zero which means the stator voltage has a constant peak amplitude. The probing frequency, Ω , needs to be selected at least 10 times smaller than the highest frequency that can pass the system without significant attenuation. The band-pass of the filters should also be less than 10% of Ω . The ES gain, k , and also a needs to be reasonably small.

The turbine power measurement is fed into the ES scheme. The optimization parameter for ES without the inner-loop control, Fig. 8, is the electrical frequency of IG stator, ω_o . Stability of system dynamics is required for convergence of ES algorithm to its peak point. It is also required that the ES algorithm operates more slowly than the WECS system dynamics. As previously mentioned, since WECS in Fig. 8 without the inner-loop controller shows a slow transient, the entire system has a lengthy convergence process which results in low power efficiency.

We employ the proposed nonlinear control to achieve the desired closed-loop performance, including faster response time (high power efficiency), and preventing magnetic saturation. Our proposed ES scheme with the inner-loop control is shown in Fig. 9. In this case, the reference inputs of the inner-loop control are ω_t^{ref} and $|\lambda|^{\text{ref}}$. We know that the MPP is parameterized by the optimal turbine speed at each

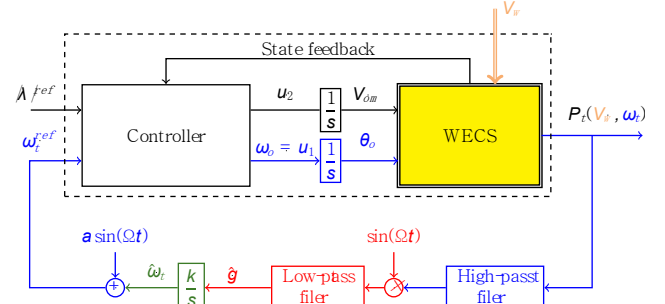


Fig. 9: The ES algorithm for MPPT of the WECS with the inner-loop control.

wind speed which is estimated by the ES loop. The other control input, $|\lambda|^{\text{ref}}$, defines the level of the flux linkage of the rotor which prevents IG from magnetic saturation.

Combination of the Controller and WECS includes fast dynamics and ES algorithm contains slow and medium speed dynamics. The ES algorithm estimates the optimal turbine speed, $\omega_t^{\text{ref}} = \omega_t^*$ which can be considered as a constant value with respect to the fast dynamics of the controller-system. The ES scheme estimates the gradient of the turbine power, P_t , by injecting a small perturbation, $a \sin(\Omega t)$, which is very slow with respect to the dynamics of the controller-system and its amplitude is enough small in comparison to ω_t . The high-pass filter removes the DC part of the signal. The multiplication of the resulting signal by $\sin(\Omega t)$ creates an estimate of the gradient of the cost function, which is smoothed using a low-pass filter. When ω_t is larger than its optimal value the estimate of the gradient, \hat{g} , is negative and causes ω_t to decrease. On the other hand, when ω_t is smaller than ω_t^* then $\hat{g} > 0$ which increases the ω_t toward ω_t^* . It should be noted that Ω is small enough in comparison to the slowest dynamic of the controller-system, with an order less than 10%.

C. Simulation Results on a Wind Turbine Model

As we mentioned earlier response time of the ES design without the inner-loop is considerably slow which results in a very low power efficiency. However, we present one simulation that compares the response of the design without the inner-loop as shown in Fig. 8 to our proposed algorithm as shown in Fig. 9 which illustrates the role of the inner-loop control. Also, we compare the performance of our proposed algorithm to the conventional algorithm including FOC and MPPT based on perturb and observe (P&O) technique.

We show a time frame of 30 s to visualize the differences between our proposed algorithm and the two other algorithms. Fig. 10 shows the wind regime applied to the WECS. The MPPT process is shown in Fig. 11. The extracted energy by our proposed algorithm is 2.36% higher than the extracted energy by the conventional MPPT and FOC. As we expected,

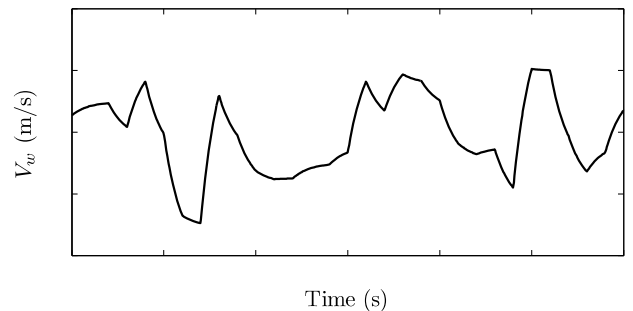


Fig. 10: Variation of wind speed versus time.

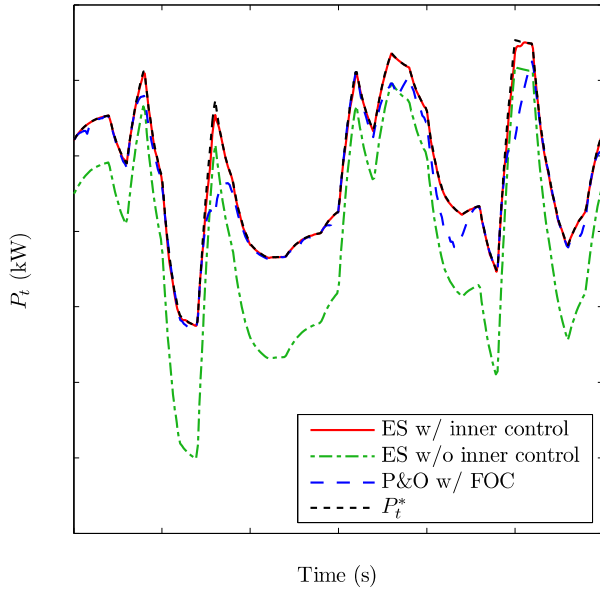


Fig. 11: MPPT, (solid red) our proposed algorithm, (dash-dot green) ES without inner-loop, (dashed blue) conventional P&O with FOC, and (dotted black) maximum power available to the WECS.

the power efficiency of the ES design without the inner-loop is low.

The proposed algorithm combines two well-known control algorithms namely, feedback linearization based on the FOC concept and extremum seeking, to achieve MPPT in a WECS operating in Region II. Our algorithm provides perfect input-output decoupling and guarantees a larger domain of attraction, which increases performance robustness with respect to the system parameters. The improved efficiency also increases the competitiveness of wind energy.

IV. PHOTOVOLTAIC SYSTEMS

Extremum seeking has been applied to MPPT design for photovoltaic (PV) micro-converter systems, where each PV module is coupled with its own DC/DC converter. Most existing MPPT designs are distributed (decentralized), i.e., they employ one MPPT loop around each converter, and all designs, whether distributed or multivariable, are gradient-based [2-4]. The convergence rate of gradient-based designs depends on the Hessian, which in turn is dependent on environmental conditions such as irradiance and temperature. Consequently, when applied to large PV arrays, the variability in environmental conditions and/or PV module degradation results in non-uniform transients in the convergence to the MPP. Using a multivariable gradient-based ES algorithm for the entire system instead of a scalar one for each PV module, while decreasing the sensitivity to the Hessian, does not eliminate this dependence [20]. We use the Newton-based ES algorithm that simultaneously employs estimates of the gradient and Hessian in the peak power tracking [19]. The convergence rate of such a design to the MPP is independent of the Hessian, with tunable transient performance that is independent of environmental conditions. We present experimental results that show the effectiveness of the proposed algorithm in comparison to existing scalar designs, and also to multivariable gradient-based ES.

Using a multivariable gradient-based ES MPPT design for the micro-converter architecture, where each PV module is coupled with its own DC/DC converter, reduces the number of required sensors (hardware reduction), and it results in more

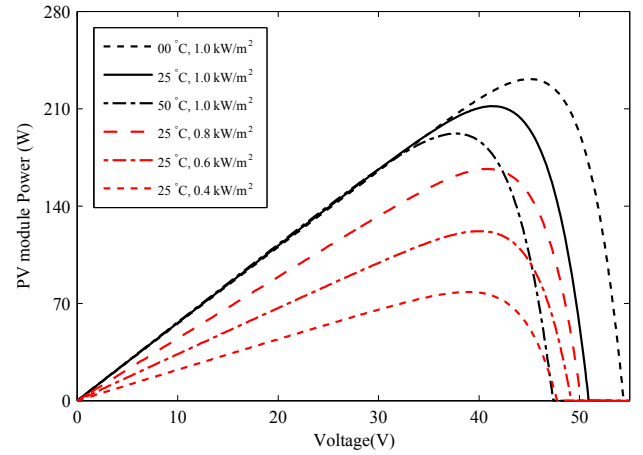


Fig. 12: Characteristic $P-V$ of a typical PV module under varying temperature and irradiance. Peak power and the optimal terminal voltage varies with change of temperature and irradiance.

uniform transients under sudden changes in solar irradiance and environmental temperature in comparison to a scalar gradient-based ES for each PV module. However, as is true of gradient-based designs, the convergence to MPP is dependent on the unknown Hessian, and varies with irradiance, temperature, and module degradation and mismatch.

In comparison with the standard gradient-based multivariable extremum seeking, the Newton-based ES removes the dependence of the convergence rate on the unknown Hessian and makes the convergence rate of the parameter estimates user-assignable. In particular, all the parameters can be designed to converge with the same speed, yielding straight trajectories to the extremum even with maps that have highly elongated level sets. When applied to the MPPT problem in PV systems, the method offers the benefit of uniform convergence behavior under a wide range of working conditions that includes temperature and irradiance variations and the non-symmetric power generation of the neighboring PV modules as a result of module degradation or mismatch.

A. Photovoltaic Modules and Power Extraction

As is clear from Fig. 12, the power-voltage ($P-V$) characteristic of a typical PV module has a unique peak (V^*, P^*) which depends on temperature and irradiance (\mathcal{T}, \mathcal{S}). It is the job of the MPPT algorithm to automatically track this MPP. In many grid-tied PV systems (including our current work), this is done by means of a separate DC/DC power electronics stage controlled by an MPPT algorithm like ES that serves two functions: (i) regulating the output DC voltage at a (near) constant value, and (ii) extracting maximum power by forcing the PV module output V to equal V^* . Fig. 13 shows this setup for a DC/DC converter stage, whose output voltage is maintained constant as V_{dc} . The ratio between the input voltage, V , and output voltage, V_{dc} , can be controlled by changing the duty cycle of the transistor switch in DC/DC converter, d , which serves as the control input.

From Fig. 12, it follows that at the MPP (V^*, P^*), the power satisfies

$$\frac{\partial P}{\partial V}(V^*) = 0, \quad \frac{\partial^2 P}{\partial V^2}(V^*) = h < 0. \quad (20)$$

An MPPT algorithm based on ES is shown for a single PV module in Fig. 13. Since $h < 0$, a positive gain, $k > 0$, guarantees the convergence of the ES toward the MPP,

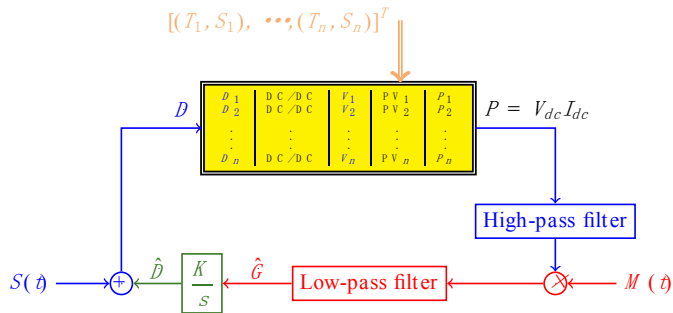


Fig. 17: Multivariable gradient-based ES for MPPT of a PV system.

In particular, the design derives an estimate \hat{G} of the gradient vector by adding the “probing signal” $S(t)$ to the estimate $\hat{D} = [\hat{D}_1 \ \hat{D}_2 \ \dots \ \hat{D}_n]^T$ of the pulse duration vector (of all the DC/DC converters). With no additional information on the Hessian (and also for simplicity), we choose the amplitudes of the probing signals to all be the same value a . It can be shown that for a proper set of ω_i for $i \in \{1, 2, \dots, n\}$, ω_l, ω_n, a , and with $K > 0$, the estimate \hat{D} of the pulse duration vector and the output P settle in a small ball around the optimal pulse duration $D^* = [D_1^* \ D_2^* \ \dots \ D_n^*]^T$ and the MPP $P(D^*)$, respectively. The radius of the ball is defined by the lowest probing frequency and its corresponding amplitude.

The linearized update equation for the estimation error $\tilde{D} = \hat{D} - D^*$ is

$$\dot{\tilde{D}} = K\tilde{D}, \quad H := \frac{\partial^2 P}{\partial D^2}(D^*), \quad (23)$$

where H is the Hessian of $P = \sum_{j=1}^n P_j$ with respect to the pulse duration vector, D .

Since the cost function P varies with irradiance, temperature, and degradation of the PV modules, so does H , and therefore a fixed adaptation gain K results in different (condition dependent) convergence rates for each converter. In order to alleviate the issue of unknown Hessian dependent convergence, we present in the next section a modified version of the multivariable Newton-based ES. In comparison with the gradient-based design of this section, the Newton-based algorithm makes the convergence rate of the parameter estimates user-assignable. In particular, all the parameters can be designed to converge with the same speed, yielding straight trajectories to the extremum even with maps that have highly elongated level sets. When applied to the MPPT problem in PV systems, the method offers the benefit of uniform convergence behavior, under a wide range of working conditions that include temperature and irradiance variations, and under the non-symmetric power generation of the neighboring PV modules as a result of module degradation or mismatch.

2) Newton-Based ES

The multivariable Newton-based ES that we propose is shown schematically in Fig. 18. As is clear from the figure, the proposed scheme extends the gradient-based ES with the estimate \hat{H} of the Hessian. The perturbation matrix $N(t)$ is defined as (9).

The goal of the Newton-based design is to replace the estimation-error dynamics $\dot{\tilde{D}} = K\tilde{D}$ with one of the form $\dot{\tilde{D}} = -K\Gamma H\tilde{D}$, where $\Gamma = H^{-1}$, that removes the dependence on the Hessian H . Calculating Γ (estimate of H^{-1}) in an algebraic fashion creates difficulties when \hat{H} is close to singularity or is indefinite. To deal with this problem, a

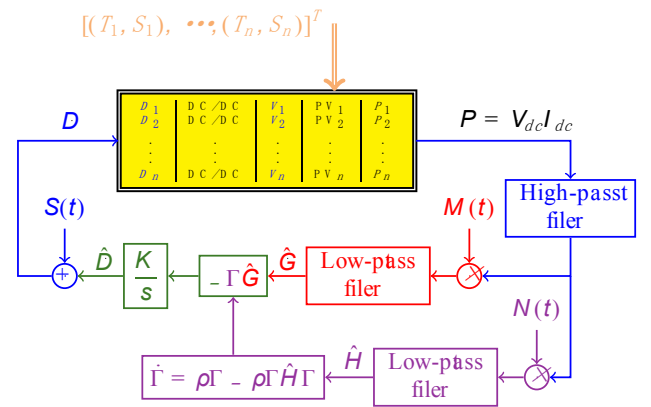


Fig. 18: Multivariable Newton-based ES for MPPT of a PV system. The purple part is added to the gradient-based ES to estimate the Hessian.

dynamic estimator is employed to calculate the inverse of \hat{H} using a Riccati equation.

Consider the following filter

$$\dot{\mathcal{H}} = -\rho\mathcal{H} + \rho\hat{H}. \quad (24)$$

Note that the state of this filter converges to \hat{H} , an estimate of H . Denote $\Gamma = \mathcal{H}^{-1}$. Since $\dot{\Gamma} = -\Gamma\mathcal{H}\Gamma$, then equation (24) is transformed into the differential Riccati equation

$$\dot{\Gamma} = \rho\Gamma - \rho\Gamma\hat{H}\Gamma. \quad (25)$$

The equilibria of the Riccati equation (25) are $\Gamma^* = 0_{n \times n}$ and $\Gamma^* = \hat{H}^{-1}$, provided \hat{H} settles to a constant. Since $\rho > 0$, the equilibrium $\Gamma^* = 0$ is unstable, whereas the linearization of (25) around $\Gamma^* = \hat{H}^{-1}$ has the Jacobian $-\rho I_{n \times n}$, so the equilibrium at $\Gamma^* = \hat{H}^{-1}$ is locally exponentially stable. This shows that, after a transient, the Riccati equation converges to the actual value of the inverse of Hessian matrix if \hat{H} is a good estimate of H .

Linearization of the update law for the error variable $\tilde{D} = \hat{D} - D^*$ results in

$$\dot{\tilde{D}} = -K\tilde{D}, \quad K > 0, \quad (26)$$

where elements of K are sufficiently small positive numbers. According to (26) the convergence rate of the parameter is independent of the shape of the cost function, and consequently, after transient, when the Hessian is close enough to its actual value, the output power converges to the MPP with the same performance regardless of environmental or mismatch conditions.

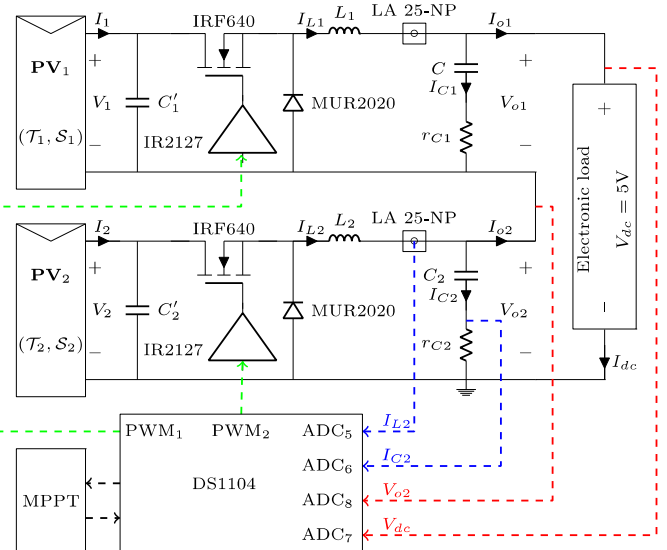


Fig. 19: Schematic of the hardware setup.



Fig. 20: Experimental setup.

D. Experimental Results

To show the effectiveness of the proposed Newton-based design in Fig. 18, and compare its performance with that of the gradient-based design in Fig. 17, we present experimental results for a PV system with $n = 2$ cascade modules.

Our hardware setup consists of 2 cascade PV modules connected to an active load which plays the role of the DC bus with $V_{dc} = 5$ V, and is schematically shown in Fig. 19. The physical hardware setup is shown in Fig. 20, and comprises of (a) custom-made PV modules constructed using 12 PV cells, (b) “Power-Pole Boards” developed by the University of Minnesota configured as DC/DC buck converters, and (c) DS1104 R&D Controller Board to implement our MPPT algorithms inside Simulink and interact with the DC/DC converters, and generate external PWM signals used by the DC/DC converters. Each Power-pole board has a current sensor LA 25-NP to measure the inductor current which we use along with the capacitor ripple current measurement to calculate the DC bus current. We employ the DC bus current and DC bus voltage to measure the power supplied to the DC bus. The selection of dSPACE hardware is intentional and it has been used as our basic experimental setup to remove the difficulties attached with hardware prototyping. As we mentioned in Introduction, the implementation of the ES algorithm is not complicated. Common electronic parts, like operational amplifiers, resistors and capacitors can be used to build an ES algorithm.

The temperature of PV modules is 25 °C and the modules are fully exposed to the sun between 0-60 s and 120-180 s. To simulate the effect of partial shading, PV₁ is covered with a plastic mat from time 60-120 s. When one module is partially shaded, the overall power level decreases. We not only compare the multivariable gradient-based and Newton-based designs, but also the traditional scalar gradient-based design, that has one MPPT loop for each converter.

Fig. 21 shows the performance of the 3 designs, and it is clear that the Newton algorithm recovers from this power level change faster than the other 2 algorithms. While the Newton method has the least steady-state error and uniform response under step down and step up power scenarios, the scalar design has the highest steady-state error and large response time in face of power decrease. The multivariable gradient-based ES performs better than the scalar MPPT under partial shading conditions.

The irradiance level of the partially shaded module is returned to normal level at $t = 120$ s. At this point the Newton scheme shows faster transient in comparison to the similar transient of the multivariable gradient-based ES and the distributed ES. The results demonstrate that the convergence rate of the Newton scheme does not vary largely from step up

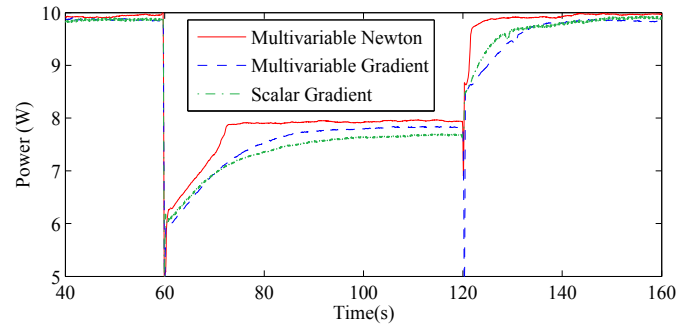


Fig. 21: Variation of power versus time. The Newton algorithm shows uniform and fast transient with low steady-state error.

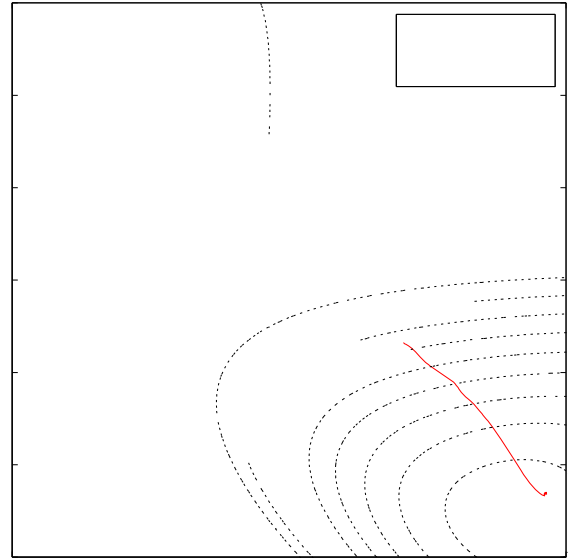


Fig. 22: Phase portrait of the MPPT for the multivariable Newton, multivariable gradient, and scalar gradient algorithms. Region (a) shows MPP area for full exposure to the sun and region (b) shows the MPP area when PV₁ is partially shaded.

to step down in power generation, which is not true for the gradient-based and distributed MPPT schemes. Not surprisingly, the experimental results are in keeping with the analytical results. Lastly, the Newton-based design moves the system in almost a straight line between extrema, in contrast to curved steepest descent trajectories of the gradient algorithm. This observation is demonstrated clearly in Fig. 22.

V. CONCLUDING REMARKS

Since environmental parameters like solar irradiance and wind speed affect the power map and maximum power point of photovoltaic (PV) and wind energy conversion systems (WECS), we propose extremum-seeking (ES), which is a model-free real-time optimization algorithm, for maximum energy harvest or maximum-power-point-tracking (MPPT) in such systems.

Extremum seeking is effective at guiding the WECS to its MPP in the sub-rated power region. However, the open-loop dynamics of the WECS have slow left half-plane poles that make the response time of the ES even slower. In order to achieve fast closed-loop response and extra features like constant voltage-to-frequency or vector control in the system, we design an inner-loop control based on the field-oriented control (FOC) concept. The combination of the inner-loop

controller and the ES algorithm improves the performance of the WECS, as shown by the simulations.

For PVs, we consider the micro-converter architecture, where each module is connected to its own DC-DC converter. Conventional designs are scalar, they: i) ignore the interaction between modules, and ii) require two (sensor) measurements per module. We propose a multivariable design that improves on each of these aspects. We consider first a multivariable gradient-based ES algorithm, where the Hessian of the power map has a dominant role in the closed-loop performance. Next, we employ a Newton-based ES algorithm, which removes the performance dependence of the gradient-based design on the Hessian. The Newton-based design has two key/distinguishing components: i) a perturbation matrix that generates the estimate of the Hessian, and (ii) a dynamic filter to estimate the inverse of the Hessian. Experimental results verify the effectiveness of the Newton-based MPPT versus its (scalar and multivariable) gradient-based counterparts.

REFERENCES

- [1] C.S. Draper and Y. T. Li, "Principles of Optimizing Control Systems and an Application to the Internal Combustion Engine", in R. Oldenburger, Ed., *Optimal and selfoptimizing control*. Boston, MA: The M.I.T. Press, 1951.
- [2] D. P. Hohm and M. E. Ropp, "Comparative study of maximum power point tracking algorithms," *Progress in Photovoltaics: Research and Applications*, vol. 11, pp. 47–62, 2003.
- [3] T. Esum and P. Chapman, "Comparison of photovoltaic array maximum power point tracking techniques," *IEEE Transactions on Energy Conversion*, vol. 22, pp. 439–449, 2007.
- [4] S. Jain and V. Agarwal, "Comparison of the performance of maximum power point tracking schemes applied to single-stage grid-connected photovoltaic systems," *IET Electric Power Applications*, vol. 1, pp. 753–762, 2007.
- [5] G. Petrone, G. Spagnuolo, M. and Vitelli, "A multivariable perturb-and-observe maximum power point tracking technique applied to a single-stage photovoltaic inverter," *IEEE Transactions on Industrial Electronics*, vol. 58, pp. 76–84, 2011.
- [6] G. Petrone, C. A. Ramos-Paja, G. Spagnuolo, and M. Vitelli, "Granular control of photovoltaic arrays by means of a multi-output Maximum Power Point Tracking algorithm", *Progress in Photovoltaics: Research and Applications*, vol. 21, pp. 918–932, 2013.
- [7] S. M. Barakati, M. Kazerani, and J. D. Aplevich, "Maximum power tracking control for a wind turbine system including a matrix converter," *IEEE Transactions on Energy Conversion*, vol. 24, pp. 705–713, 2009.
- [8] S. M. R. Kazmi, H. Goto, H.-J. Guo, and O. Ichinokura, "A novel algorithm for fast and efficient speed-sensorless maximum power point tracking in wind energy conversion systems," *IEEE Transaction on Industrial Electronics*, vol. 58, pp. 29–36, 2011.
- [9] M. Krstic and H.-H. Wang, "Stability of extremum seeking feedback for general nonlinear dynamic systems," *Automatica*, vol. 36, pp. 595–601, 2000.
- [10] J.-Y. Choi, M. Krstic, K. B. Ariyur, and J. S. Lee, "Extremum seeking control for discrete-time systems," *IEEE Trans. Automat. Contr.*, vol. 47, pp. 318–323, 2002.
- [11] K. B. Ariyur, and M. Krstic, *Real-Time Optimization by Extremum Seeking Feedback*, Wiley-Interscience, 2003.
- [12] Y. Tan, D. Netic, I. and Mareels, "On non-local stability properties of extremum seeking control," *Automatica*, vol. 42, pp. 889–903, 2006.
- [13] A. Ghaffari, M. Krstic, and D. Netic, "Multivariable Newton-based extremum seeking," *Automatica*, vol. 48, pp. 1759–1767, 2012.
- [14] H.-H. Wang, S. Yeung, and M. Krstic, "Experimental application of extremum seeking on an axial-flow compressor," *IEEE Trans. Contr. Syst. Technol.*, vol. 8, pp. 300–309, 2000.
- [15] A. Banaszuk, K. B. Ariyur, M. Krstic, and C. A. Jacobson, "An adaptive algorithm for control of combustion instability," *Automatica*, vol. 40, pp. 1965–1972, 2004.
- [16] R. Becker, R. King, R. Petz, and W. Nitsche, "Adaptive closed-loop separation control on a high-lift configuration using extremum seeking," *AIAA Journal*, vol. 45, pp. 1382–1392, 2007.
- [17] C. Zhang, D. Arnold, N. Ghods, A. Siranosian, and M. Krstic, "Source seeking with nonholonomic unicycle without position measurement and with tuning of forward velocity," *Systems & Control Letters*, vol. 56, pp. 245–252, 2007.
- [18] D. Carnevale, A. Astolfi, C. Centioli, S. Podda, V. Vitale, and L. Zaccarian, "A new extremum seeking technique and its application to maximize RF heating on FTU," *Fusion Engineering and Design*, vol. 84, pp. 554–558, 2009.
- [19] A. Ghaffari, M. Krstic, and S. Seshagiri, "Power optimization for photovoltaic micro-converters using multivariable Newton-based extremum-seeking," in *Proc. of IEEE Conference on Decision and Control*, 2012.
- [20] A. Ghaffari, S. Seshagiri, and M. Krstic, "Power optimization for photovoltaic micro-converters using multivariable gradient-based extremum-seeking," in *Proc. of American Control Conference*, 2012.
- [21] A. Ghaffari, M. Krstic, and S. Seshagiri, "Power Optimization and Control in Wind Energy Conversion Systems using Extremum Seeking", *Proc. of American Control Conference*, 2013.
- [22] K. E. Johnson, L. Y. Pao, M. J. Balas, and L. J. Fingersh, "Control of variable-speed wind turbines: standard and adaptive techniques for maximizing energy capture," *IEEE Control Systems Magazine*, vol. 26, pp. 70–81, 2006.
- [23] R. Cardenas, R. Pena, J. Clare, and P. Wheeler, "Analytical and experimental evaluation of a WECS based on a cage induction generator fed by a matrix converter," *IEEE Transactions on Energy Conversion*, vol. 26, pp. 204–215, 2011.
- [24] R. Marino, S. Peresada, and P. Valigi, "Adaptive input-output linearizing control of induction motors," *IEEE Transactions on Automatic Control*, vol. 38, pp. 208–221, 1993.